



Hierarchical Load Tracking Control of a Grid-connected Solid Oxide Fuel Cell for Maximum Electrical Efficiency Operation

Li, Yonghui ; Wu, Qiuwei; Zhu, Haiyu

Published in:
Energies

Link to article, DOI:
[10.3390/en8031896](https://doi.org/10.3390/en8031896)

Publication date:
2015

[Link back to DTU Orbit](#)

Citation (APA):

Li, Y., Wu, Q., & Zhu, H. (2015). Hierarchical Load Tracking Control of a Grid-connected Solid Oxide Fuel Cell for Maximum Electrical Efficiency Operation. *Energies*, 8(3), 1896-1916. <https://doi.org/10.3390/en8031896>

General rights

Copyright and moral rights for the publications made accessible in the public portal are retained by the authors and/or other copyright owners and it is a condition of accessing publications that users recognise and abide by the legal requirements associated with these rights.

- Users may download and print one copy of any publication from the public portal for the purpose of private study or research.
- You may not further distribute the material or use it for any profit-making activity or commercial gain
- You may freely distribute the URL identifying the publication in the public portal

If you believe that this document breaches copyright please contact us providing details, and we will remove access to the work immediately and investigate your claim.

7 **Hierarchical Load Tracking Control of a Grid-connected Solid**
8 **Oxide Fuel Cell for Maximum Electrical Efficiency Operation**

9 **Yonghui Li**^{1,*}, **Qiuwei Wu**^{2,†}, **Haiyu Zhu**^{3,†}

10 ¹ School of Electrical Engineering of Wuhan University, Wuhan 430072, China;

11 ² Center for Electric Power and Energy, Department of Electrical Engineering, Technical University
12 of Denmark, Kgs. Lyngby, 2800 Denmark; Email: qw@elektro.dtu.dk;

13 ³ Wuhan Guoce Science & Technology Co., Ltd, Wuhan 430223, China; E-mail: zhuhaiyu@gmail.com

14 [†] These authors contributed equally to this work.

15 * Author to whom correspondence should be addressed; E-Mail: lyhwhu@163.com;

16 Tel.: +86-27-68774230; Fax: +86-27-68774230.

17 External Editor:

18 *Received: / Accepted: /*

19 *Published:*

20

21 **Abstract:** Based on the benchmark solid oxide fuel cell (SOFC) dynamic model for power
22 system studies and the analysis of the SOFC operating conditions, the nonlinear
23 programming (NLP) optimization method was used to determine the maximum electrical
24 efficiency of the grid-connected SOFC subject to the constraints of fuel utilization factor,
25 stack temperature and output active power. The optimal operating conditions of the grid-
26 connected SOFC were obtained by solving the NLP problem considering the power
27 consumed by the air compressor. With the optimal operating conditions of the SOFC for
28 the maximum efficiency operation obtained at different active power output levels, a
29 hierarchical load tracking control scheme for the grid-connected SOFC was proposed to
30 realize the maximum electrical efficiency operation with the stack temperature bounded.
31 The hierarchical control scheme consists of a fast active power control and a slower stack
32 temperature control. The active power control was developed by using a decentralized
33 control method. The efficiency of the proposed hierarchical control scheme was
34 demonstrated by case studies using the benchmark SOFC dynamic model.

35

36 **Keywords:** Hierarchical control scheme; maximum electrical efficiency; nonlinear
 37 programming; solid oxide fuel cell
 38

39 Nomenclature

40 Symbols

41	a	V	Tafel constant
42	b	V	Tafel slope
43	$c_i(s)$		The i^{th} controller
44	C_p	J.mol ⁻¹ K ⁻¹	Molar constant-pressure heat capacity
45	E_0	V	Nernst potential at standard pressure
46	E	V	Nernst potential
47	F	96485C.mol ⁻¹	Faraday constant
48	$g(s)$		Transfer function
49	h	J.mol ⁻¹	Molar enthalpy
50	I_{FC}	A	Stack current
51	I_L	A	Limiting current
52	k	3.762	Mole ratio of nitrogen to oxygen in the air
53	K_i	mol.s ⁻¹ .Pa ⁻¹	The i^{th} gas valve molar constant
54	m		Modulation index
55	$m_s C_{ps}$	J.K ⁻¹	Stack solid mass-specific product
56	N_0		Cell number in series
57	N		Mole number
58	p	MPa	Stack operating pressure
59	P	kW	Fuel cell output power
60	P_{loss}	kW	Power loss caused by the air compressor
61	q	mol.s ⁻¹	Mole flow rate
62	R	8.314J K ⁻¹ mol ⁻¹	Universe gas constant
63	T	K	Temperature
64	u		Fuel utilization factor
65	V	m ³	Electrode volume
66	V_{dc}	V	Cell terminal voltage
67	V_s	V	Grid bus voltage
68	Greek letters		
69	α	Ω	Ohmic resistant constant
70	β	K	Ohmic resistant constant
71	δ	rad	Phase shift angle
72	η		SOFC electrical efficiency
73	η_c		Air compressor efficiency
74	ρ		Multiplicate model factor

75	τ	s	Time constant
76	ϕ		Dynamic Relative Index
77	Subscripts		
78	a		Anode
79	c		Cathode
80	H_2		Hydrogen
81	H_2O		Water
82	N_2		Nitrogen
83	O_2		Oxygen
84	std		Standard
85	Superscripts		
86	in		<i>Inlet</i>
87	r		<i>Reacted</i>
88	out		<i>Outlet</i>

89 1. Introduction

90 It is a trend to replace conventional power plants by the more environmentally-friendly distributed
 91 generators (DG) in order to reduce the greenhouse gas (GHG) emission from the power sector. Among
 92 the various types of DG, the high-temperature solid oxide fuel cell (SOFC) is one of the viable options
 93 due to its relatively high electrical efficiency of 45%-65% compared to typically 30-35% efficiency in
 94 conventional power plants [1,2]. Furthermore, high temperature reaction heat produced during the
 95 energy conversion process in the fuel cell (FC) stack permits an SOFC generator to be coupled to a gas
 96 turbine to form a combined heat and power (CHP) system, which can reach higher efficiency of up to
 97 80% [3,4].

98 Various cell operating variables such as output power, stack temperature and fuel utilization factor,
 99 among others, do affect the thermodynamic, mass transfer, electrochemical and electrical processes
 100 within the SOFC in complex and intricate manners [5]. In the literature, researchers studied the
 101 possible effects of operating variables on the efficiency of different types of FC [6-8]. From these
 102 studies, it is shown that it is important but difficult to determine the optimal operating condition of the
 103 FC operation in order to achieve the maximum efficiency.

104 Therefore, like wind turbine, photovoltaic and other kind of renewable sources [9], a controller must
 105 be carefully designed in order to ensure that the SOFC power plant operates at the maximum
 106 efficiency for tracking the external power demand. Some references have made a comprehensive
 107 review of the SOFC modeling and control [10-12]. The SOFC dynamic models range from zero-
 108 dimensional (0-D) to three-dimensional (3-D). Both 2-D and 3-D models can be used for the cell
 109 geometrical design and thermal stress analysis [13-15]. These models are able to accurately represent
 110 the behavior of the FC at the expense of a heavy computational burden and are not suitable for power
 111 system studies. The 0-D and 1-D models are for the control purposes such as steady state and transient
 112 performance prediction and optimization. Most of the 1-D models are used for the stand-alone SOFC
 113 analysis. It was reported in [16] that the SOFC stack terminal voltage and temperature will reach a
 114 steady state value after a few seconds and tens of minutes respectively under the constant fuel

115 utilization factor control scheme when the stack current has a step change. In order to mitigate the
116 temperature excursion and extend the cell material lifespan, the excess air for cooling can be adjusted
117 by a proportional-integral (PI) controller, a variable structure controller or a neural network predictive
118 controller [17-19]. Komatsu et al studied the transient response of the SOFC for load tracking. The PI
119 controllers considering the constraints of temperature, fuel utilization factor and steam-to-carbon ratio
120 were proposed based on the feedback control [20]. It is shown that the response time of the stack
121 terminal voltage and temperature after a step change of the dc output power is very close to what have
122 been reported in [16]. 0-D SOFC models have been widely used for load tracking studies under both
123 stand-alone and grid-connected conditions [21-23]. Such a lumped-parameter model can emulate the
124 FC operations with acceptable accuracy only if certain strict assumptions are met, e.g. the fuel
125 utilization factor is constant [11]. With regard to the control of a SOFC, model predictive control
126 (MPC) [24] and adaptive control [25] can achieve multiple objectives during the load tracking process.
127 Sendjaja and Kariwala [26] studied the use of decentralized proportional-integral-derivative (PID)
128 controllers on the benchmark constant temperature SOFC dynamic model given in [21]. The same
129 benchmark model was used in [27] and [28] to study the load tracking and small-signal stability issues
130 pertaining to a grid-connected SOFC. As the stack temperature has been recognized to have significant
131 impacts on the cell lifespan, some studies have improved the constant temperature model by including
132 the energy balance equation. It was reported in [29-31] that the temperature can be maintained within a
133 safe range by regulating the air flow rate. Vijay et al showed that the response of the stack temperature
134 is in the order of several minutes when the stack current has a step change [30]. Some control schemes
135 examined in [30] were found to be suitable for the decentralized controller design although the
136 maximum electrical efficiency operations of the SOFC had not been considered. Bunin et al in [31]
137 provided the experimental validation of a strategy to achieve the optimal efficiency operation of a
138 stand-alone SOFC. The experimental results verified the simulation studies in [16] and [20]. Without
139 considering the possible power losses consumed by the auxiliary devices, the optimal efficiency of the
140 SOFC reported in [31] is between 40% and 50% over the power range. When the SOFC is connected
141 to an external ac power system through a power control unit (PCU), the active power control of the
142 PCU shall be taken into account as well in order to achieve the maximum efficiency load tracking
143 operation and has not been studied.

144 The paper presents a maximum electrical efficiency load-tracking control scheme for the grid-
145 connected SOFC in order to improve the operation performance. In Section 2, by using an existing
146 benchmark SOFC dynamic model specifically developed for power system studies, the maximum
147 efficiency of the SOFC can be obtained by solving a non-linear programming problem which is subject
148 to a set of steady-state equality and inequality constraints. Next, the locations of the open-loop poles of
149 the dynamic model lead to the proposed structure of the hierarchical control scheme shown in Section
150 3. In order to achieve the optimal operating state, a decentralized power and temperature control
151 system is proposed and described in Section 4. The performance of the maximum electrical efficiency
152 load tracking control scheme is illustrated through the case studies in Section 5, followed by the
153 conclusions.

154 **2. Determination of the Optimal Operating Condition of a Grid-connected SOFC Using** 155 **Nonlinear Programming**

In order to facilitate the analysis, the following assumptions are made,

- (1) Hydrogen rich nature gas is converted to hydrogen (H₂) through the external-reforming fuel processor. Like in [22], the carbon oxide (CO) shift reaction is ignored in the analysis. Only pure H₂ is fed to the anode;
- (2) Oxygen in the air is used as the oxidant. The mole ratio of nitrogen (N₂) to oxygen (O₂) in the air is denoted as k_c which is 3.762;
- (3) Both the fuel and air are preheated to the same temperature before they are transmitted to the cell stack. The detailed thermal management is not studied;
- (4) The cell stack is well-insulated and the energy losses caused by radiation, convection and conduction are negligible.

2.1. The SOFC Dynamic Model for Power System Studies

Padullés et al [21] developed one of the earliest SOFC stack models specifically for power system studies, and the model is shown within the dash lines in Figure 1. In this model, it is assumed the stack temperature T is constant. Considering the cell stack tabular structure, the channels that transport the gases along the electrodes have a fixed volume, but their lengths are small. Hence it is sufficient to define one single pressure value in the cell stack interior. The exhaust of each channel is via a single orifice. The ratio of pressures between the interior and exterior of the channel is large enough and it can be assumed that the orifice is choked and the lumped-parameter model can be derived. Therefore, the mass balance equation, expressed in terms of the partial pressures p_i , is given as,

$$\frac{dp_i}{dt} = \frac{RT}{V_i}(q_i^{in} - q_i^o - q_i^r) = \frac{1}{\tau_i} \left[\frac{1}{K_i}(q_i^{in} - q_i^r) - p_i \right] \quad (1)$$

where the subscript ' i ' denotes either H₂, O₂ or water (H₂O), the superscript ' in ', ' o ' and ' r ' denote the input, output and reaction variable, respectively, R is the ideal gas constant, V_i is the anode or cathode volume, and q_i , K_i and τ_i are the i^{th} gas mole flow rate, valve molar constant and time constant, respectively. Thus, τ_i can be written as,

$$\tau_i = V_i / (K_i RT) \quad (2)$$

According to the Faraday's Law of Electrolysis, the reaction flow rates are,

$$q_{H_2}^r = 2q_{O_2}^r = -q_{H_2O}^r = 2K_r I_{FC} \quad (3)$$

where $K_r = N_0 / (4F)$, N_0 is the number of the cells connected in series in the stack, F is the Faraday constant of 96485 C.mol⁻¹, and I_{FC} is the stack current.

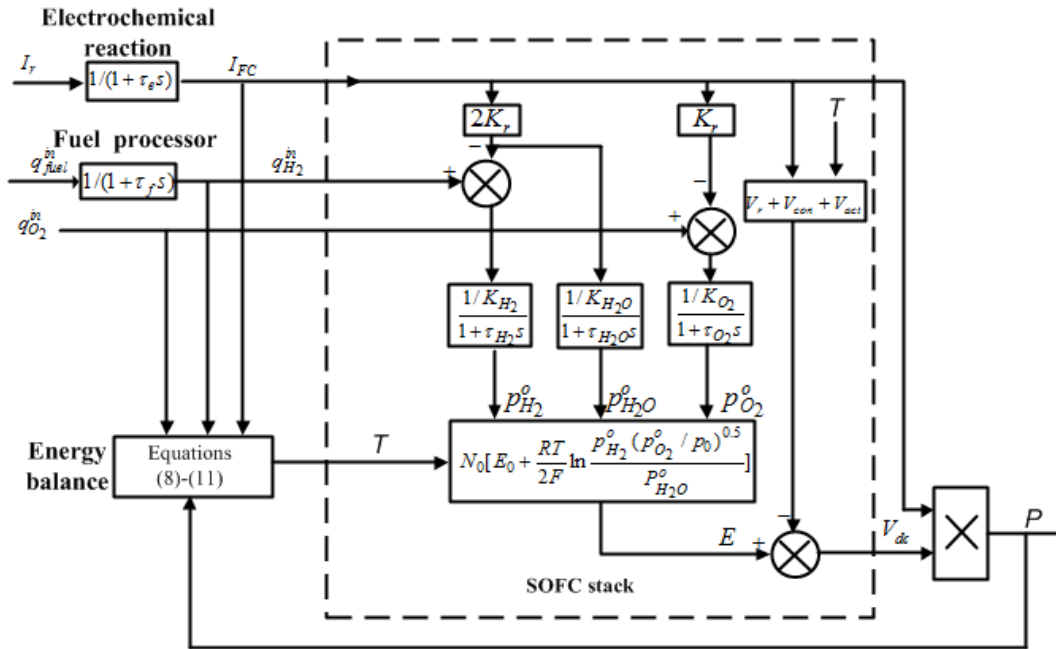
In order to improve the SOFC model, Zhu and Tomsovic included the dynamics of the electrochemical reaction and the fuel processor [22]. In Figure 1, these processes are represented by two first-order equations,

$$dI_{FC} / dt = (I_r - I_{FC}) / \tau_e \quad (4)$$

$$dq_{H_2}^{in} / dt = (q_{fuel}^{in} - q_{H_2}^{in}) / \tau_f \quad (5)$$

185 where I_r is the reference stack current, q_{fuel}^{in} is the natural gas input, τ_e and τ_f are the respective process
 186 time constants.

187 **Figure 1.** The benchmark SOFC dynamic model.



188
 189
 190 It can be seen from (1)–(2) that the partial pressures p_i are dependent on the stack temperature T
 191 which has to be carefully controlled as it can affect the cell efficiency, stack reliability and lifespan [5].
 192 In order to improve the accuracy of the stack model, the dynamic behavior of the cell according to T
 193 can be derived based on the energy balance principle [30]. The relevant equation is,

$$m_s C_{ps} dT / dt = \sum q_i^{in} (\bar{h}_i^{in} - \bar{h}_i^o) + \sum q_i^r \bar{h}_i^o - P \quad (6)$$

194 where P is the SOFC dc output power, $m_s C_{ps}$ is the mass-specific heat product of the stack, \bar{h}_i is the i^{th}
 195 gas per mole enthalpy and it can be written as,

$$\bar{h}_i = \bar{h}_{i,std} + \bar{C}_{pi} \Delta T \quad (7)$$

196 In (7), $\bar{h}_{i,std}$ is the i^{th} gas per mole enthalpy at the standard pressure of 0.1MPa and the standard
 197 temperature T_{std} of 283K, \bar{C}_{pi} is the i^{th} gas average constant-pressure specific heat and ΔT is the
 198 temperature change.

199 Substituting (3) and (7) into (6), (6) can be rewritten as,

$$dT / dt = (A / B - T - P / B) / \tau_T \quad (8)$$

200 where

$$A = [\bar{C}_{pH_2} q_{H_2}^{in} + (\bar{C}_{pO_2} + k_c \bar{C}_{pN_2}) q_{O_2}^{in}] T_{in} - K_r I_{FC} T_{std} (2\bar{C}_{pH_2} q_{H_2}^{in} + \bar{C}_{pO_2} - 2\bar{C}_{pH_2O}) - 2K_r I_{FC} H_{LHV} \quad (9)$$

From Figures 1 and 2, it is seen that the grid-connected SOFC power plant has four control variables, namely q_{fuel}^{in} , $q_{O_2}^{in}$, m and δ . As Q is strongly dependent on m , m is therefore often manipulated to allow the SOFC power plant to operate under constant voltage, constant reactive power or constant power factor operating schemes. The present investigation, however, focuses on the active power control. Accordingly, the SOFC power plant terminal is treated as a PV bus. In addition, if the switching losses in the PCU and in the feeder are ignored, I_{FC} can be regulated through m and δ [27],

$$I_{FC} = mkV_s \sin \delta / X \quad (14)$$

2.3. Operating Variables and Constraints

The operating variables of the grid-connected SOFC such as T , V_{dc} , P , $q_{H_2}^{in}$, $q_{O_2}^{in}$ and I_r (I_{FC}) can be calculated based on the energy balance principle, Nernst equation and Figure 1, *i.e.* through solving the following equations,

$$\sum q_i^{in}(\bar{h}_i^{in} - \bar{h}_i^o) + \sum q_i^r \bar{h}_i^o = P \quad (15)$$

$$V_{dc} = N_0 \left[E_0 + \frac{RT}{2F} \ln \frac{p_{H_2}^o (p_{O_2}^o / p_0)^{0.5}}{p_{H_2O}^o} \right] - V_{act} - V_r - V_{con} \quad (16)$$

$$P = V_{dc} I_{FC} \quad (17)$$

where E_0 , the ideal standard potential, is a function of T [30],

$$E_0 = 1.2856 + 0.000252T \quad (18)$$

In (16), p_0 is the standard pressure. V_{act} , V_r and V_{con} , as shown in (19)–(21), are activation loss, Ohmic loss and concentration loss, respectively [1]. The detailed definitions of the parameters and their typical values are given in Nomenclature and Table 1

$$V_{act} = a + b \log I_{FC} \quad (19)$$

$$V_r = \alpha \exp[\beta(1/T_{in} - 1/T)] I_{FC} \quad (20)$$

$$V_{con} = RT/(2F) \cdot \ln(1 - I_{FC}/I_L) \quad (21)$$

Among the six steady-state operating variables T , V_{dc} , P , $q_{H_2}^{in}$, $q_{O_2}^{in}$ and I_r (I_{FC}), if any three of them are given, the other three can be obtained by solving the nonlinear equations (15)–(17).

The cell lifespan and performance are dependent on the operating parameters. Therefore, three operating constraints must be respected for the safe operation of the cell. The most important operating constraint is the fuel utilization factor u , given as,

$$u = 2K_r I_{FC} / q_{H_2}^{in} \quad (22)$$

$$u_{min} \leq u \leq u_{max} \quad (23)$$

Typically $u_{min} = 0.7$ and $u_{max} = 0.9$ [21].

The other two operating constraints are T and P ,

$$T_{min} \leq T \leq T_{max} \quad (24)$$

$$P_{\min} \leq P \leq P_{\max} \quad (25)$$

243 Typically, $T_{\min} = 1173\text{K}$, $T_{\max} = 1273\text{K}$, $P_{\min} = 0.1\text{pu}$ and $P_{\max} = 1\text{pu}$ of the SOFC rated power [1,23].

244 2.4. Determination of the Optimal Operating Condition

245 The electrical efficiency η of the hydrogen SOFC is defined as the ratio of the net power to the total
246 power obtainable by burning H_2 at the standard state [1],

$$\eta = (P - P_{\text{loss}}) / (q_{\text{H}_2}^{\text{in}} H_{\text{LHV}}) \quad (26)$$

247 However, if the stack operating pressure p is higher than 0.1MPa, not all the power generated by the
248 SOFC will be delivered to the external circuit. The parasitic losses P_{loss} is dominated by the air
249 compressor in the form [1],

$$P_{\text{loss}} = \bar{C}_{\text{pair}} T_{\text{std}} (p^{0.286} - 1)(1 + k_c) q_{\text{O}_2}^{\text{in}} / \eta_c \quad (27)$$

250 where η_c is the equivalent efficiency of the air compressor.

251 Under a given pressure p , it can be seen from (26) and (27) that η is the function of P , $q_{\text{H}_2}^{\text{in}}$ and $q_{\text{O}_2}^{\text{in}}$.

252 There is one set of operating variables which enables the SOFC to operate at the maximum electrical
253 efficiency η_{max} . In order to optimize η , a nonlinear programming problem (NLPP) is formulated as
254 follows,

255 Objective function

$$\text{Maximize } \eta \quad (28)$$

256 Subject to

$$\begin{aligned} & \text{Equality constraints (15)-(17)} \\ & \text{Inequality constraints (23)-(25)} \end{aligned} \quad (29)$$

257 The optimization is obtained by treating P , $q_{\text{H}_2}^{\text{in}}$ and $q_{\text{O}_2}^{\text{in}}$ as the decision variables in the NLPP.
258 Numerical optimization software packages such as that provided by MATLAB can be used to search
259 η_{max} . At the end of the NLPP search, the optimal set of T , V_{dc} , $q_{\text{O}_2}^{\text{in}}$, $q_{\text{H}_2}^{\text{in}}$, I_r (I_{FC}) as well as u for a
260 targeted P will be obtained and pre-stored in a look-up table as the reference input signals for the
261 SOFC load tracking control system.

262 3. Hierarchical Load Tracking Control Scheme for the Grid-connected SOFC

263 With the optimal operating condition of the SOFC determined by the NLPP, the load tracking
264 control scheme for the grid-connected SOFC can be developed to track the power demand and operate
265 at η_{max} .

266 The open-loop poles of the SOFC are analyzed to study the dynamic response of the SOFC and a
267 hierarchical control scheme for the SOFC is proposed based on the dynamic response analysis.

268 3.1. Analysis of the Open-loop System Poles

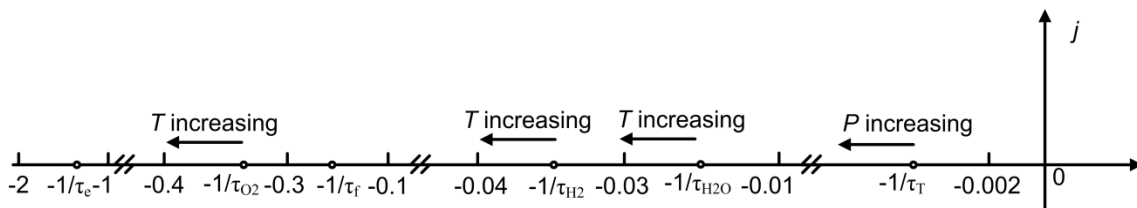
269 In the load tracking control scheme for the SOFC, the internal dynamics of the PCU can be
 270 neglected as the typical response time of the PCU is a few milliseconds. The load tracking speed of the
 271 SOFC will be dominated by the dynamic response of devices on the dc side of the power plant where
 272 the typical time constants are of the order of 1s or larger.

273 The response characteristics of the SOFC operating at the maximum efficiency can be assessed by
 274 examining the locations of the six open-loop poles of the dynamic model shown in Figure 1. The i^{th}
 275 pole can be calculated as,

$$s_i = -1/\tau_i \tag{30}$$

276 The electrochemical reaction and fuel processor contribute to the poles $-1/\tau_e$ and $-1/\tau_f$. They are
 277 independent of P and T . However, the location of the poles $-1/\tau_{H_2}$, $-1/\tau_{O_2}$, $-1/\tau_{H_2O}$ and $-1/\tau_T$ may change
 278 when the SOFC operates at different power levels. As shown in (2) and Figure 3, three gas time
 279 constants are the function of T but independent of I_{FC} . Therefore, $-1/\tau_{H_2}$, $-1/\tau_{O_2}$ and $-1/\tau_{H_2O}$ will be
 280 away from the origin when T increases. On the other hand, from (10) and (11), τ_T is seen to be
 281 inversely proportional to I_{FC} . Thus, the remaining pole $-1/\tau_T$ is directly proportional to I_{FC} or P .

282 **Figure 3.** Illustrative of the positions of the six poles of the dynamic model



283
 284 When the SOFC operates at η_{max} , the poles can be divided into two groups: plotted in Figure 3, the
 285 distance of the pole $-1/\tau_T$ to the imaginary axis is at least six times smaller than that of the other five
 286 poles. The observation on the locations of the open-loop poles shall be used to develop the structure of
 287 the hierarchical load tracking and temperature control scheme for the SOFC.

288 **3.2. The Hierarchical Load Tracking Control Scheme**

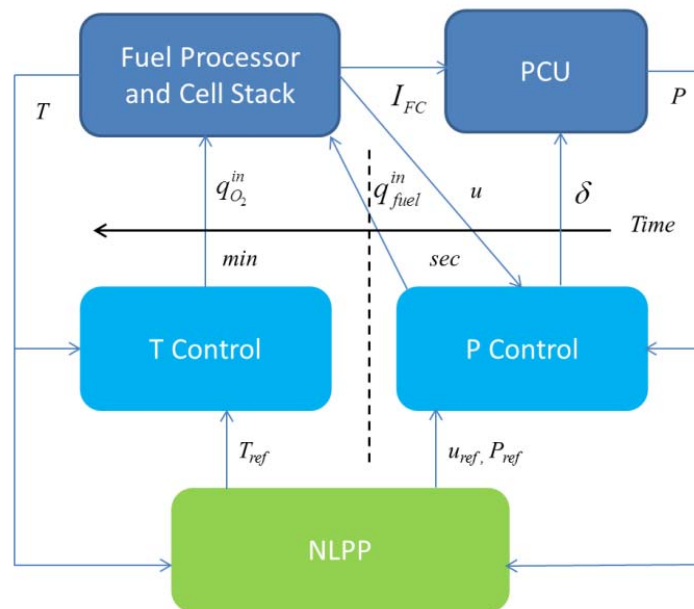
289 Figure 2 shows that q_{fuel}^{in} , $q_{O_2}^{in}$, m and δ can be used to regulate the SOFC output active and reactive
 290 power. In the design of a control system for a multi-input-multi-output plant, it is desirable that the
 291 structure of the control system is selected in such a way that possible interactions between the control
 292 loops is minimized. The modulation index m of the PCU can be used to control the bi-directional
 293 reactive power flow to the grid and this can be accomplished in a few milliseconds. Therefore, among
 294 the four control variables, m can be treated as a quasi-steady state variable during the load tracking
 295 process because the electrochemical, mass transfer and thermodynamics processes usually takes a
 296 much longer period.

297 Based on the observation on the locations of the open-loop poles, it can be concluded that the pole $-$
 298 $1/\tau_T$ essentially governs the dynamics of the stack temperature T whereas the load tracking process is
 299 dominated by the remaining poles. The T control typically lasts for tens of seconds. Therefore, T can
 300 be assumed to be constant for the load tracking operation. On the other hand, by adopting the practice
 301 of [29-31] in which O_2 was used as a coolant to regulate T , the oxygen flow rate $q_{O_2}^{in}$ can be

manipulated such that T is maintained at the optimal value to realize the SOFC η_{max} operation. It therefore results in a single-input-single-output (SISO) stack temperature control scheme, denoted as the T control system in this paper. With the T control in place, the remaining two control variables q_{fuel}^{in} and δ can be utilized to perform the load tracking of P while maintaining u at the optimal value. This strategy leads to a two-input-two-output P control system.

In summary, as shown in Figure 4, a hierarchical control structure is proposed to achieve both the maximum electrical efficiency operation and stack temperature control of the SOFC when the FC tracks the power demand. The structure is based on the inherent differences in the speeds of response of P , u and T of the SOFC to the demand changes. P and u can be controlled by regulating the control variables q_{fuel}^{in} and δ while T is to be controlled through regulating $q_{O_2}^{in}$, subject to the operating constraints (23)-(25). The proposed hierarchical control structure is more comprehensive, in comparison with the on-line load tracking scheme shown in [27] in which T is assumed constant.

Figure 4. Diagram of the hierarchical control scheme



315

316 4. Design of the P and T Control Systems

317 The detailed design procedure of the P and T control systems is described in this section.

318 4.1. SOFC Dynamic Model for the Design of P Controller

319 According to Section 3.2, T can be assumed constant during the P control process. Therefore, the nonlinear model given in Figure 1 can be linearized around the plant initial operating state. For the convenience of the analysis and controller design, the plant variables are normalized in the following way. The values of the state variables $q_{fuel,max}^{in}$, u_{max} , P_{max} , δ_{max} , which correspond to the operating condition when the SOFC operates at the maximum P , are selected as the base for the normalization. The normalized output-control model shall be of the form

324

$$y(s) = G_p(s)w(s) = \begin{pmatrix} g_{P\delta}(s) & g_{Pf}(s) \\ g_{u\delta}(s) & g_{uf}(s) \end{pmatrix} w(s) \quad (31)$$

325 where $y = [\Delta P, \Delta u]^T$ and $w = [\Delta \delta, \Delta q_{fuel}^{in}]^T$ are the small deviations of the output and control variables. $G_p(s)$
 326 is the transfer function determined by taking the small signal form of (1), (4), (5), (14), (16)-(22).
 327 Algebraic manipulation shall yield the following expressions for the various elements in $G_p(s)$:

$$g_{P\delta}(s) = \left[P_0 + \frac{I_{r,0}^2 (g_E - g_V)}{1 + \tau_e s} \right] \frac{ctg \delta_0 \delta_{max}}{P_{max}} \quad (32)$$

$$g_{Pf}(s) = \frac{RT_0 u_0}{1 - u_0} \frac{1}{(1 + \tau_e s)(1 + \tau_f s)} \frac{q_{fuel,max}^{in}}{P_{max}} \quad (33)$$

$$g_{u\delta}(s) = \frac{u_0 ctg \delta_0 \delta_{max}}{1 + \tau_e s} \frac{\delta_{max}}{u_{max}} \quad (34)$$

$$g_{uf}(s) = \frac{-u_0^2}{2K_r I_{r,0}} \frac{1}{1 + \tau_e s} \frac{q_{fuel,max}^{in}}{u_{max}} \quad (35)$$

328 where

$$g_E(s) = -\frac{N_0 RT_0}{2F} \left(\frac{2K_r}{q_{fuel,0}^{in} - 2K_r I_{r,0}} \frac{1}{1 + \tau_{H_2} s} + \frac{1}{I_{r,0}} \frac{1}{1 + \tau_{H_2O} s} + \frac{K_r}{2(q_{O_2,0}^{in} - K_r I_{r,0})} \frac{1}{1 + \tau_{O_2} s} \right) \quad (36)$$

$$g_V(s) = \frac{b}{I_{r,0}} + \alpha \exp\left[\beta\left(\frac{1}{T_{in}} - \frac{1}{T_0}\right)\right] - \frac{RT_0}{2F} \frac{1}{I_L - I_{r,0}} \quad (37)$$

329 The subscript '0' in (32)-(37) indicates the initial value of the respective variables when the SOFC
 330 operates at η_{max} .

331 4.2. Selection of P Control Output-input Variables Pairs

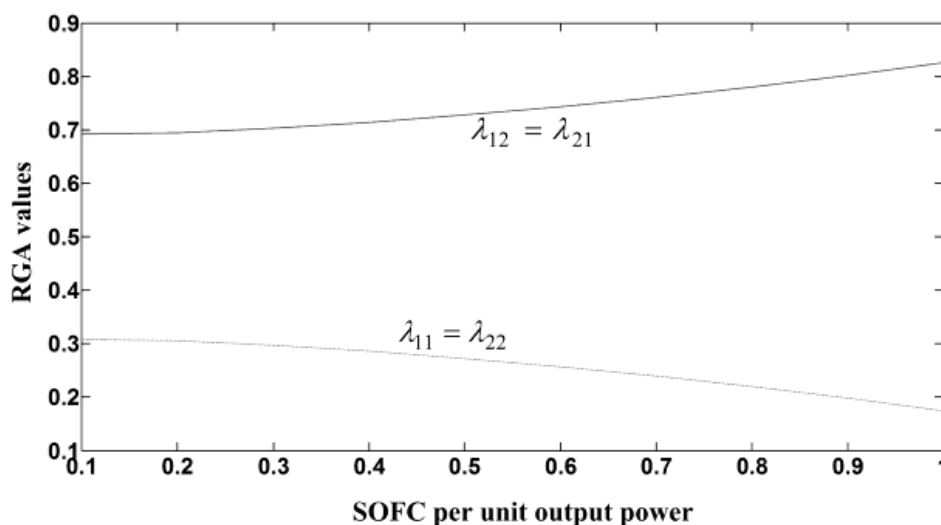
332 Although there are many methods of designing a control system for a general two-input-two-output
 333 plant, the decentralized control is a widely used approach. The advantages of the decentralized control
 334 include hardware simplicity, operation flexibility, and the relative ease in the controller design and
 335 tuning. However, the dynamic performance of the resulting two SISO sub-systems may be degraded
 336 by any unaccounted interactions between the two control loops. Therefore, in order to design a feasible
 337 and robust controller, an important step is to determine the most suitable two output-input variable
 338 pairs for the two SISO sub-systems.

339 The relative gain array (RGA) is an established technique to measure the steady-state interactions
 340 between multiple SISO loops [32]. In the design of the P control system, there are two possible
 341 selections of output-input variable pairs: the $(P - \delta, u - q_{fuel}^{in})$ pair and the $(P - q_{fuel}^{in}, u - \delta)$ pair. The
 342 most suitable output-input variables pair shall be examined by observing the relative steady state gain
 343 between the inputs and outputs. Define the RGA matrix Λ of the plant (31) as the Hadamard product of
 344 $G_p(0)$ and its inverse transposition,

$$\Lambda = G_p(0) \circ G_p^{-T}(0) \quad (38)$$

345 With the typical values given in Table 1 and the SOFC operating at η_{max} , the variations of each
 346 element of Λ are shown in Figure 5. It is shown that the values of the off-diagonal elements λ_{12} and λ_{21}
 347 are closer to 1 compared to that of the diagonal elements λ_{11} and λ_{22} , particularly under heavy load
 348 conditions. This means the selection of the output-input pair $(P-q_{fuel}^{in}, u-\delta)$ will be more suitable
 349 because the interactions of the $P-\delta$ and $u-q_{fuel}^{in}$ loops are smaller and decreases as P increases.
 350 Therefore, $(P-q_{fuel}^{in}, u-\delta)$ were selected as the output-input variable pairs when designing the P control
 351 system.

352 **Figure 5.** Variations of the values of Λ elements with P .



353

354 4.3. Design of the Decentralized P Controller

355 Figure 6(a) shows the P control block diagram where an input variable with the subscript ‘*ref*’
 356 denotes its reference value. The figure has been configured to reflect the outcome of the pair selection
 357 described in the previous sub-section, *i.e.* the adoption of the $(P-q_{fuel}^{in}, u-\delta)$ output-input variable pairs.
 358 The system of Figure 6(a) is then split into two independent SISO systems, with each SISO having the
 359 structure shown in Figure 6(b). The so-called multiplicate model factor (MMF) is utilized to account
 360 for the loop interactions between the two SISO systems. In Figure 6(b), $c_i(s)$ is the respective controller
 361 where the subscript “*i*” denotes either P or u . The design method for $c_i(s)$ can be summarized as
 362 follows.

363 **Step One:** Design the $c_i(s)$ controllers without considering loop interactions. Suppose the controller
 364 $c_i(s)$ in Figure 6(b) is the PID type and is tuned using the simple internal mode control (SIMC) method
 365 described in [32]. Thus for a second-order system $g_{ii}(s)$ with a dc-gain k_i and a time delay θ_i :

$$g_{ii}(s) = k_i e^{-\theta_i s} [(\tau_i s + 1)(\tau_i' s + 1)]^{-1}; \tau_i > \tau_i'; \theta_i > 0 \quad (39)$$

366 $c_i(s)$ shall be of the form,

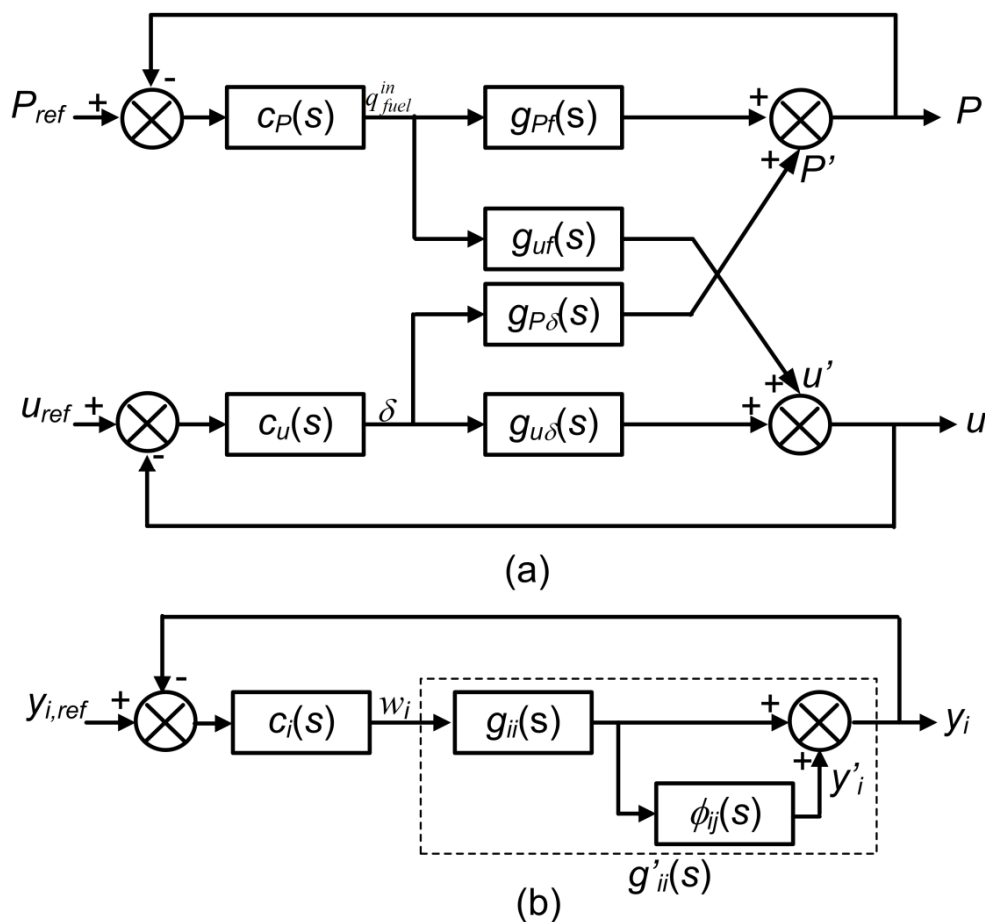
$$c_i(s) = k_{pi} (1 + 1/\tau_{ii} s)(1 + \tau_{di} s) \quad (40)$$

367 It can be seen from (33) and (34) that in $g_{Pf}(s)$ and $g_{u\delta}(s)$, $\theta_i=0$. Set the desired closed-loop cross-
 368 over time constant τ_{ci} equals to τ_{ii} , a practice often used in the process control [32], the PID parameter
 369 settings are then given as,

$$k_{pi} = 1/k_i; \tau_{ii} = \tau_i; \tau_{di} = \tau_i' \tag{41}$$

370 With this set of settings, the phase margin of $c_i(s)g_{ii}(s)$ is 90° and it meets the typically desirable
 371 phase margin of 60° . While it can be seen from (33) that $g_{Pf}(s)$ is independent of P , however, (34)
 372 shows the dc-gain of $g_{u\delta}(s)$ will be the maximum when $P = P_{min}$. Therefore, the $c_u(s)$ controller must be
 373 designed based on the minimum SOFC output power condition.

374 **Figure 6.** P control as applied to: (a) the two-input-two-output SOFC plant model, (b) the
 375 individual decentralized SISO plant model.



376

377 **Step Two:** Calculate the MMF by using dynamic Relative Index (dRI) and obtain the equivalent
 378 transfer function of each SISO system. In Figure 6(b), it is shown the output of the sub-system i will be
 379 superimposed by the output y'_i from the neighboring system j . Define the dRI between y'_i and the
 380 output of the subsystem i as $\phi_{ij}(s)$. $\phi_{ij}(s)$ for the P control system can then be derived using the
 381 technique described in [32] for a general process system,

$$\phi_{ij}(s) = -g_{ij}(s)g_{ji}(s)g_{ii}^{-1}(s)(c_j^{-1}(s) + g_{jj}(s))^{-1} \tag{42}$$

382 The MMF of the i^{th} SISO system is then given as,

$$\rho_i(s) = 1 + \phi_{ij}(s) = |\rho_i| e^{-\Delta\theta_i s} \quad (43)$$

383 $|\rho_i|$ and $\Delta\theta_i$ are the magnitude and phase angle of the MMF, respectively. Therefore, the rectangular
 384 box formed by the delineated lines in Figure 6(b) represents the equivalent transfer function $g'_{ii}(s)$
 385 where

$$g'_{ii}(s) = \rho_i(s) g_{ii}(s) = |\rho_i| k_i e^{-(\theta_i + \Delta\theta_i)s} [(\tau_i s + 1)(\tau'_i s + 1)]^{-1} \quad (44)$$

386 In (44), $|\rho_i|$ and $\theta_i + \Delta\theta_i$ vary with the operating condition of the SOFC. $g'_{ii}(s)$ can be chosen under
 387 the most onerous conditions when both $|\rho_i|$ and $\theta_i + \Delta\theta_i$ have the maximum values, although maximum
 388 $|\rho_i|$ and $\theta_i + \Delta\theta_i$ may not necessarily occur under the same operating condition. With this practice,

$$\rho_{i,\max} = \max(1, |\rho_i|); \theta_{i,\max} = \max(\theta_i + \Delta\theta_i) \quad (45)$$

389 **Step Three:** Redesign each $c_i(s)$ based on the equivalent transfer function $g'_{ii}(s)$. In a manner
 390 similar to that in designing the SIMC-PID controller in Step One, if the time constant corresponding to
 391 the closed-loop cross-over frequency of $c_i(s)g'_{ii}(s)$ is selected to be the same as the process maximum
 392 time constant τ_{ci} , as suggested in [32], the new controller settings for $c_i(s)$ are,

$$k_{pi} = \tau_i / [|\rho_{i,\max}| k_i (\tau_{ci} + \theta_{i,\max})]; \tau_{ii} = \min(\tau_i, 4(\tau_{ci} + \theta_{i,\max})); \tau_{di} = \tau'_i \quad (46)$$

393 4.4. T Control System Design

394 As explained in Section 3.2, the temperature control involves slower dynamics of the hierarchical
 395 control system. Since the SOFC output power P can be maintained at the targeted value through the
 396 regulation of the faster P - q_{fuel}^{in} and u - δ control loops, P can be assumed to have reached a quasi-steady
 397 state value, even before the T control loop starts to become active. From (8)-(11) and Figure 1,
 398 selecting $q_{O_2,\max}^{in}$ and T_{min} as the normalization base, the small-signal perturbation equation of the
 399 temperature T is,

$$\Delta T(s) = g_{T_o}(s) \Delta q_{O_2}^{in} = \frac{(\bar{C}_{pO_2} + k_c \bar{C}_{pN_2})(T_{in} - T_0) q_{O_2,\max}^{in}}{m_s C_{ps} s + B} \frac{1}{T_{min}} \Delta q_{O_2}^{in} \quad (47)$$

400 Last equation indicates that at steady-state, an increase in $q_{O_2}^{in}$ will lead to a decrease in T because
 401 $T_{in} < T_0$. However, as explained in Section 2, the parameter B will increase when I_{FC} increases. As B
 402 also appears in the denominator of (47), the consequence is that the phase margin of the transfer
 403 function $g_{T_o}(s)$ in (47) will be at the minimum when I_{FC} is at the minimum, *i.e.* when $P = P_{min}$.
 404 Therefore, the parameters of the temperature controller $c_T(s)$ can be determined using the same SIMC-
 405 PID tuning method as that used in the design of the P controller. $c_T(s)$ is to be tuned under the most
 406 onerous condition when the SOFC is at the minimum load.

407 4.5. Overall Load Tracking and Temperature Control Scheme

408 The overall control scheme for the SOFC to achieve η_{max} during the load tracking process is
 409 illustrated in the ‘‘Control and Optimization System’’ portion of Figure 2. Based on the above analysis,

410 both P and u will be ahead of T to reach the reference values. It can be seen from (8) and will be
 411 illustrated in Section 5 that continuously varying P may lead the transient T to exceed the constraint
 412 given in (24). In order to guarantee the cell lifespan, T should be monitored on-line. If the measured T
 413 is not within the pre-set band which is close to its operating boundaries, as shown in Figure 2, the “Pre-
 414 filter” block will convert the error between the targeted power level P_t and the SOFC output power P
 415 into continuous adjustments P_{ref} . Since the overall control objective of the load tracking is to achieve
 416 η_{max} , the reference signals T_{ref} and u_{ref} can be obtained directly from the look-up table. Hence the
 417 SOFC shall attempt to operate at η_{max} as it approaches P_t . The hierarchical control scheme will track
 418 P_{ref} , u_{ref} and T_{ref} through the respective controllers $c_P(s)$, $c_u(s)$ and $c_T(s)$.

419 5. Case Studies

420 The benchmark SOFC power plant in [21, 22, 30] was used to carry out case studies to illustrate the
 421 efficiency of the proposed hierarchical control scheme. The 100kW power plant is connected to a
 422 400V ac system and the associated parameters are given in Table 1. On the 400V and 100kVA base,
 423 the SOFC power plant ac terminal voltage is assumed to be constant at 1.05pu. It is also assumed that
 424 the link reactance X in Figure 2 is 0.05pu. The simulation tool used is MATLAB/SIMULINK.

425 5.1. Steady-state η_{max} Operations

426 Suppose the SOFC is to operate between 10kW and 100kW. Table 2 shows part of the NLPP
 427 calculation results. For comparison, like the steady-state operating conditions in [26] and [27], the
 428 efficiencies (η_l) when $T=1273K$ and $u=0.8$ under different power are also given. Obviously, η_{max} is
 429 higher than η_l . The optimal η can be found on the boundaries of T and u when P is at the low level.
 430 The highest η_{max} is 43.4% when $P=0.3pu$. However, the power consumed by the air compressor is over
 431 15% of the output power if the cell operating pressure is 0.15MPa. This will cause η_{max} less than 40%
 432 under the maximum output power condition.

433 **Table 1.** Typical 100kW SOFC power plant data

Parameters	Value
T_{in}	923K
p	0.15MPa
N_0	384
$m_s C_{ps}$	1.1×10^4 (J/K)
K_r	9.95×10^{-4} mol/(s.A)
K_{H2}	8.32×10^{-6} mol/(s.Pa)
K_{H2O}	2.77×10^{-6} mol/(s.Pa)
K_{O2}	2.49×10^{-5} mol/(s.Pa)
V_a	$2.3m^3$
V_c	$0.76m^3$
τ_f	5s
τ_e	0.8s
α	0.02 Ω
β	-2870K

b	0.11V
a	0.05V
I_L	800A
η_c	0.7

434 5.2. Controller Design

435 For the controllers design, the u_{max} , P_{max} , δ_{max} , $q_{fuel,max}^{in}$, $q_{O_2,max}^{in}$ and T_{min} are chosen as 0.9, 100kW,
436 0.05rad, 0.872mol/s, 2.187mol/s and 1173K.

437 Based on the analysis in Section 4.2, the P control system is split into two SISO sub-systems.
438 Analysis in Section 4.3 has identified the minimum output power condition to be the most onerous
439 condition. From (40), if the cross-over time constant of each SISO system is set equal to the maximum
440 τ_{ii} , the controllers for the P control designed without considering the loop interactions are $c_P(s) =$
441 $1.237(1+1/5s)(1+0.8s)$ and $c_u(s) = 0.095(1+1/0.8s)$. This design corresponds to the cross-over time
442 constants of 0.2s and 1.25s for the $P - q_{fuel}^{in}$ loop and $u - \delta$ loop, respectively.

443 **Table 2.** The maximum efficiency results by NLPP

P (kW)	P_{loss} (kW)	V_{dc} (V)	q_{fuel}^{in} (mol/s)	$q_{O_2}^{in}$ (mol/s)	$T(K)$	u	η_{max}	η_l
10	1.514	269.31	0.082	0.208	1173	0.9	0.427	0.3904
30	4.438	272.06	0.244	0.610	1173	0.9	0.434	0.3973
50	7.560	269.49	0.410	1.040	1173	0.8998	0.428	0.3992
70	10.889	266.08	0.585	1.497	1173	0.8948	0.418	0.3988
90	14.416	261.51	0.771	1.982	1175	0.8885	0.406	0.3973
100	15.906	257.87	0.872	2.187	1184	0.8849	0.399	0.395

444 When P is 0.1pu or 1pu, the corresponding dRI are: $\phi_{P\delta,0.1}(j0.2) = 1.414\angle 16.1^\circ$; $\phi_{P\delta,1}(j0.2) =$
445 $0.634\angle -28.6^\circ$; $\phi_{uf,0.1}(j1.25) = 0.443\angle 9.5^\circ$; and $\phi_{uf,1}(j1.25) = 0.423\angle 13.6^\circ$. The values of $\phi_{P\delta,P}(\cdot)$ confirm
446 the most onerous condition under which the $P - q_{fuel}^{in}$ loop interact with the $u - \delta$ loop is at the minimum
447 P condition. The values of $\phi_{uf,P}(\cdot)$ show that this loop can contribute to the $P - q_{fuel}^{in}$ loop with the
448 largest gain increase, and the maximum phase lag under the minimum and the maximum P conditions,
449 respectively. In order to guarantee satisfactory dynamic performance of the SOFC under possible loop
450 failures for all output power conditions, the corresponding MMF can be selected to be the extreme gain
451 and phase values simultaneously. Thus, based on the above numerical results and using (43), $\rho_{P\delta} =$
452 $2.391\exp(-0.96s)$ and $\rho_{uf} = 1.442\exp(0.04s)$. The corresponding equivalent transfer function of each
453 SISO system can then be calculated using (44) and (45) to yield $g'_{P\delta}(s) = 1.839\exp(-$
454 $0.96s)/((1+1/5s)(1+0.8s))$ and $g'_{u\delta}(s) = 15.147/(1+0.8s)$. From (46), the new P controllers are $c_P(s)$
455 $= 0.531(1+1/5s)(1+0.8s)$ and $c_u(s) = 0.066(1+1/0.8s)$.

456 As discussed in Section 4.4, the controller for the T control system is also designed when $P = P_{min}$.
457 Accordingly, the T controller is $c_T(s) = -0.64(1+1/292s)$.

458 Again, the above three controllers designed for the model shown in Figure 1 indicate the SOFC is
459 feasible for slow load tracking application. The tracking speed is firstly limited by the P controllers. As
460 the cross-over time constant of $c_P(s)$ is around 0.2s, it will be safe for the SOFC to track the load

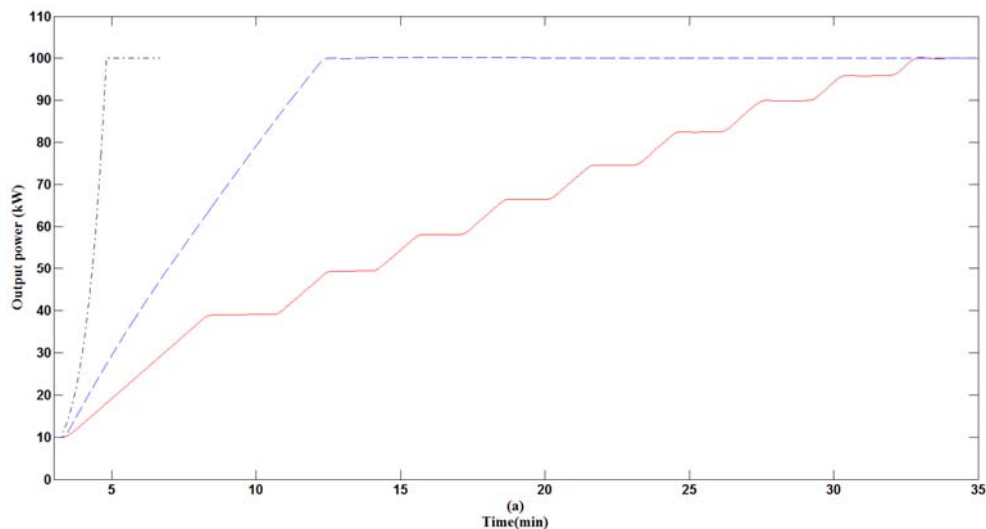
461 within this bandwidth. On the other hand, the cross-over time constant of $c_T(s)$ is about 0.0035s. The T
 462 control system is much slower than the P control system. As shown in (8), the continuing output power
 463 change will cause T deviate from the acceptable value. Therefore, the load tracking speed must be slow
 464 down until T can be effectively regulated within the constraints.

465 5.3. SOFC Load Tracking Dynamic Performance

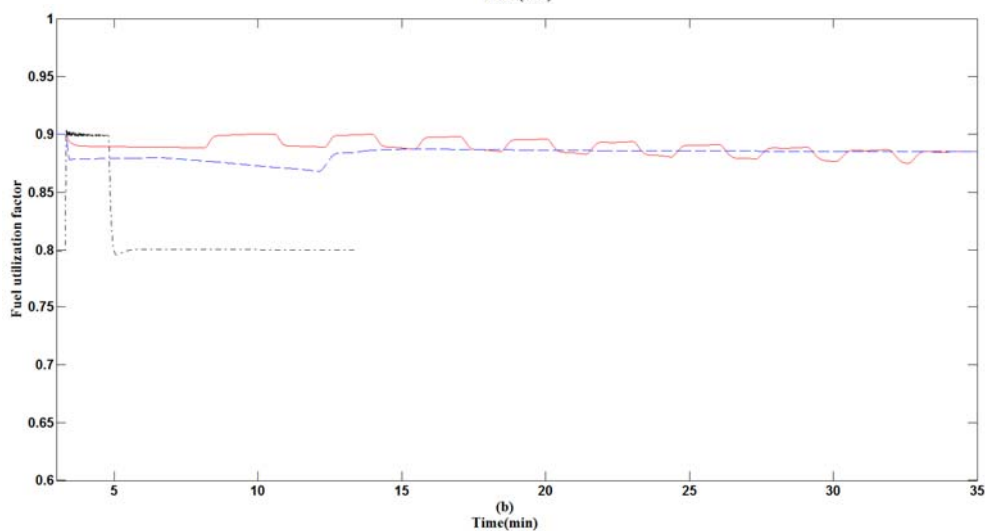
466 This section illustrates the load tracking performance of the SOFC under the proposed hierarchical
 467 control scheme with and without considering the temperature control. The results are then compared
 468 with that obtained from the on-line control scheme described in [27]. Suppose the power demand
 469 increases from 0.1pu to 1pu. If the measured T is within the constraints, the load demand on the SOFC
 470 can change at the rate of 0.1 pu kW/min. Such load tracking speed is quite close to the results reported
 471 in [20] and [31]. However, as discussed in Section 4.3 and shown in Figure 7a, the “Pre-filter” block
 472 can generate the new power reference only the measured T is below a pre-set threshold value (say
 473 1263K). It will take about 30 minutes to achieve the targeted power due to the variable power ramp
 474 rate. If the temperature control is not considered, the targeted power can be reached in about 12
 475 minutes. The on-line control strategy proposed in [27] is designed such that the final load level shall be
 476 reached within the minimum time. Indeed, the on-line method shown in Figure 7(a) has a higher speed
 477 of response, *i.e.* the 0.9pu power change is reached in about 100s. However, in [27], the ratio of the
 478 fuel flow rate to oxygen flow rate is kept constant at 1.145. It is shown in Table 2 that it is impossible
 479 to maintain a constant T with the flow rate ratio fixed. Therefore, the constant temperature assumption
 480 made in [27] is invalid once the energy balance consideration is included in the dynamic model.

481 An interesting observation is that the direction of the u variation based on the on-line method is
 482 opposite to that obtained under the hierarchical control. This is shown in Figure 7(b). The reason for
 483 this is because under the on-line scheme proposed in [27], q_{fuel}^{in} is the only independent control variable
 484 and u is kept constant at a pre-set value (which, in this simulation, is 0.8). As derived in [27], q_{fuel}^{in} and
 485 u will vary in the same direction following the load change. Under the hierarchical control scheme,
 486 however, both q_{fuel}^{in} and δ will affect u . Due to the loop interactions, u will vary in a direction opposite
 487 to that of q_{fuel}^{in} , as shown in (35). However, the hierarchical control scheme can achieve the optimal
 488 value 0.8849, as can be seen in the figure.

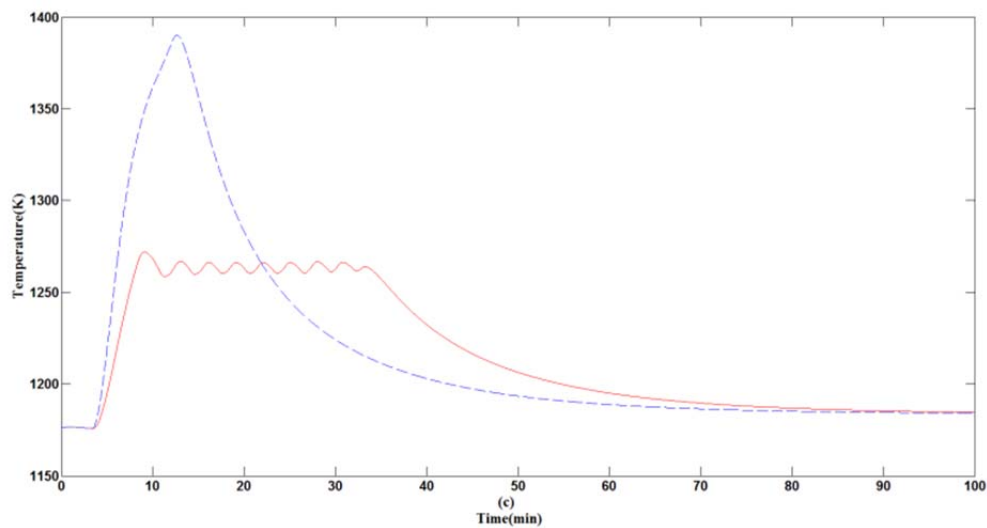
489 **Figure 7.** Comparison of SOFC load tracking performance under hierarchical control
 490 scheme with considering T bound (—), hierarchical control scheme without considering T
 491 bound (---) and on-line control scheme of [27] (-.)



492



493



494

495 From the initial optimal value 1173K, Figure 7c indicates that it will take about 90 minutes for the
 496 SOFC to reach at 1184K. T can be maintained under 1273K during the transient period if T bound is
 497 satisfied with the variable load tracking speed. Otherwise, T will be out of the constraint due to the
 498 continuously increasing P .

499 According to the discussion above, it can be concluded that the proposed hierarchical control
500 scheme will be able to track the power demand in a safe manner, and the mutual loop interactions have
501 been included in the control system design. The scheme will also lead to the maximum electrical
502 efficiency operations of the SOFC.

503 6. Conclusions

504 By considering the power loss caused by the air compressor, the maximum electrical efficiency
505 operating conditions of the grid-connected SOFC can be obtained by solving a nonlinear programming
506 problem which is subject to constraints of stack temperature, fuel utilization factor and output power.
507 In order to accommodate the inherently different dynamical processes within the SOFC, a hierarchical
508 control scheme for the grid-connected SOFC power plant has been proposed. The scheme consists of a
509 P control system and a relatively slower T control system. The case studies verify that the proposed
510 hierarchical control scheme can achieve maximum efficiency load tracking operation for the grid-
511 connected SOFC with the stack temperature bounded within the preset constraints.

512 The FC-based DG technology is still far from mature. Continuous improvements on the FC
513 performance, durability and making it economically competitive are needed in order to realize its wide
514 application. For power system analysis, the SOFC model and control strategies should be improved
515 and verified through experiment in the future work.

516 Conflicts of Interest

517 The authors declare no conflict of interest.

518 References

- 519 1. Larminie, J.; Dicks, A. Fuel cell system explained. 2nd ed.; John Wiley: New York, 2002.
- 520 2. Singhal, S.C.; Kendall, K. High temperature solid oxide fuel cells: Fundamentals, design, and
521 applications. Elsevier: New York, 2003.
- 522 3. Zhang, X.; Chan, S.H.; Li, G.; Ho, H.K.; Li, J.; Feng, Z. A review of integration strategies for
523 solid oxide fuel cells. *Journal of Power Sources* 2010, 195, 685-702.
- 524 4. Park, S.K.; Ahn, J.-H.; Kim, T.S. Performance evaluation of integrated gasification solid oxide
525 fuel cell/gas turbine systems including carbon dioxide capture. *Applied Energy* 2011, 88, 2976-
526 2987.
- 527 5. Razbani, O.; Wærnhus, I.; Assadi, M. Experimental investigation of temperature distribution over
528 a planar solid oxide fuel cell. *Applied Energy* 2013, 105, 155-160.
- 529 6. Zhu, G.-R.; Loo, K.H.; Lai, Y.M.; Tse, C.K. Quasi-maximum efficiency point tracking for direct
530 methanol fuel cell in dmfc-supercapacitor hybrid energy system. *IEEE Trans. Energy Convers.*
531 2012, 27, 561-571.
- 532 7. Kelouwani, S.; Adegnon, K.; Agbossou, K.; Dube, Y. Online system identification and adaptive
533 control for pem fuel cell maximum efficiency tracking. *IEEE Trans. Energy Convers.* 2012, 27,
534 580-592.

- 535 8. Hong, W.-T.; Yen, T.-H.; Chung, T.-D.; Huang, C.-N.; Chen, B.-D. Efficiency analyses of
536 ethanol-fueled solid oxide fuel cell power system. *Applied Energy* 2011, 88, 3990-3998.
- 537 9. Su, Y.; Chan, L.-C.; Shu, L.; Tsui, K.-L. Real-time prediction models for output power and
538 efficiency of grid-connected solar photovoltaic systems. *Applied Energy* 2012, 93, 319-326.
- 539 10. Bhattacharyya, D.; Rengaswamy, R. A reiview of solid oxide fuel cell (sofc) dynamic model. *Ind.*
540 *Eng. Chem. Res.* 2009, 48, 6068-6086.
- 541 11. Wang, K.; Hissel, D.; Péra, M.C.; Steiner, N.; Marra, D.; Sorrentino, M.; Pianese, C.;
542 Monteverde, M.; Cardone, P.; Saarinen, J. A review on solid oxide fuel cell models. *International*
543 *Journal of Hydrogen Energy* 2011, 36, 7212-7228.
- 544 12. Huang, B.; Qi, Y.; Murshed, M. Solid oxide fuel cell: Perspective of dynamic modeling and
545 control. *Journal of Process Control* 2011, 21, 1426-1437.
- 546 13. Spivey, B.J.; Edgar, T.F. Dynamic modeling, simulation, and mimo predictive control of a tubular
547 solid oxide fuel cell. *Journal of Process Control* 2012, 22, 1502-1520.
- 548 14. Menon, V.; Janardhanan, V.M.; Tischer, S.; Deutschmann, O. A novel approach to model the
549 transient behavior of solid-oxide fuel cell stacks. *Journal of Power Sources* 2012, 214, 227-238.
- 550 15. Gao, F.; Simoes, M.G.; Blunier, B.; Miraoui, A. Development of a quasi 2-d modeling of tubular
551 solid-oxide fuel cell for real-time control. *IEEE Trans. Energy Convers.* 2014, 29, 9-19.
- 552 16. Wang, C.; Nehrir, M.H. A physically based dynamic model for solid oxide fuel cells. *IEEE Trans.*
553 *Energy Convers.* 2007, 22, 887-897.
- 554 17. Sorrentino, M.; Pianese, C.; Guezennec, Y.G. A hierarchical modeling approach to the simulation
555 and control of planar solid oxide fuel cells. *Journal of Power Sources* 2008, 180, 380-392.
- 556 18. Huo, H.B.; Wu, Y.X.; Liu, Y.Q.; Gan, S.H.; Kuang, X.H. Control-oriented nonlinear modeling
557 and temperature control for solid oxide fuel cell. *Journal of Fuel Cell Science and Technology*
558 2010, 7.
- 559 19. Hajimolana, S.A.; Tonekabonimoghadam, S.M.; Hussain, M.A.; Chakrabarti, M.H.; Jayakumar,
560 N.S.; Hashim, M.A. Thermal stress management of a solid oxide fuel cell using neural network
561 predictive control. *Energy* 2013, 62, 320-329.
- 562 20. Komatsu, Y.; Kimijima, S.; Szmyd, J.S. Numerical analysis on dynamic behavior of solid oxide
563 fuel cell with power output control scheme. *Journal of Power Sources* 2013, 223, 232-245.
- 564 21. Padulles, J.; Ault, G.W.; McDonald, J.R. An integrated sofc plant dynamic model for power
565 systems simulation. *Journal of Power Sources* 2000, 86, 495-500.
- 566 22. Zhu, Y.; Tomsovic, K. Development of models for analyzing the load-following performance of
567 microturbines and fuel cells. *Electric Power Systems Research* 2002, 62, 1-11.
- 568 23. Li, Y.H.; Choi, S.S.; Rajakaruna, S. An analysis of the control and operation of a solid oxide fuel-
569 cell power plant in an isolated system. *IEEE Trans. Energy Convers.* 2005, 20, 381-387.
- 570 24. Li, Y.G.; Shen, J.; Lu, J.H. Constrained model predictive control of a solid oxide fuel cell based
571 on genetic optimization. *Journal of Power Sources* 2011, 196, 5873-5880.
- 572 25. Nayeripour, M.; Hoseintabar, M. A new control strategy of solid oxide fuel cell based on
573 coordination between hydrogen fuel flow rate and utilization factor. *Renewable and Sustainable*
574 *Energy Reviews* 2013, 27, 505-514.

- 575 26. Sanandaji, B.M.; Vincent, T.L.; Colclasure, A.M.; Kee, R.J. Modeling and control of tubular
576 solid-oxide fuel cell systems: Ii. Nonlinear model reduction and model predictive control. *Journal*
577 *of Power Sources* 2011, 196, 208-217.
- 578 27. Li, Y.H.; Rajakaruna, S.; Choi, S.S. Control of a solid oxide fuel cell power plant in a grid-
579 connected system. *IEEE Trans. Energy Convers.* 2007, 22, 405-413.
- 580 28. Du, W.; Wang, H.F.; Zhang, X.F.; Xiao, L.Y. Effect of grid-connected solid oxide fuel cell power
581 generation on power systems small-signal stability. *IET Renewable Power Generation* 2012, 6,
582 24.
- 583 29. Sorrentino, M.; Pianese, C. Model-based development of low-level control strategies for transient
584 operation of solid oxide fuel cell systems. *Journal of Power Sources* 2011, 196, 9036-9045.
- 585 30. Vijay, P.; Tade, M.O.; Datta, R. Effect of the operating strategy of a solid oxide fuel cell on the
586 effectiveness of decentralized linear controllers. *Ind. Eng. Chem. Res.* 2011, 50, 1439-1452.
- 587 31. Bunin, G.A.; Wuillemin, Z.; Francois, G.; Nakajo, A.; Tsikonis, L.; Bonvin, D. Experimental real-
588 time optimization of a solid oxide fuel cell stack via constraint adaptation. *Energy* 2012, 39, 54-
589 62.
- 590 32. Wang, Q.G.; Ye, Z.; Cai, W.J.; Hang, C.C. *Pid control for multivariable processes*. Springer:
591 Berlin, 2009.